

Spontaneous Mechanical and Electrical Activities of Human Calf Musculature at Rest Assessed by Repetitive Single-Shot Diffusion-Weighted MRI and Simultaneous Surface Electromyography

Authors

Martin Schwartz^{1,2*}, Günter Steidle¹, Petros Martirosian¹, Ander Ramos-Murguialday^{3,4}, Hubert Preißl^{5,6}, Alto Stemmer⁷, Bin Yang², Fritz Schick¹

Affiliation

- 1: Section on Experimental Radiology, University of Tübingen, Tübingen, Germany
- 2: Institute of Signal Processing and System Theory, University of Stuttgart, Stuttgart, Germany
- 3: Institute for Medical Psychology and Behavioural Neurobiology, University of Tübingen, Tübingen, Germany
- 4: Neurotechnology Laboratory, TECNALIA Health Department, San Sebastian, Spain
- 5: Institute for Diabetes Research and Metabolic Diseases of the Helmholtz Centre Munich at the University of Tuebingen, German Centre for Diabetes Research (DZD), Tübingen, Germany
- 6: Department of Pharmacy and Biochemistry, Institute of Pharmaceutical Sciences, Interfaculty Centre for Pharmacogenomics and Pharma Research, University of Tübingen, Tübingen, Germany
- 7: Siemens Healthcare GmbH, Erlangen, Germany

Corresponding Author*

Martin Schwartz, Section on Experimental Radiology, Hoppe-Seyler-Str. 3, 72076 Tübingen, Germany. Fon: +49-7071-29-80495. E-Mail: martin.schwartz@med.uni-tuebingen.de

Running title

Simultaneous surface EMG and DWI of SMAM

Number of words

5419

Key Words: Spontaneous Mechanical Activities in Musculature, Surface Electromyography, Diffusion-Weighted Imaging, Incoherent Motion

Abstract

Purpose: Assessment of temporal and spatial relations between spontaneous mechanical activities in musculature (SMAM) at rest as revealed by diffusion-weighted imaging (DWI) and electrical muscular activities in surface EMG (sEMG). Potential influences of static and radio-frequency (RF) magnetic fields on muscular activity on sEMG measurements at rest were examined systematically.

Methods: Series of diffusion-weighted stimulated echo planar imaging were recorded with concurrent sEMG measurements. Electrical activities in sEMG were analyzed by non-parametric Friedman and two-sample Kolmogorov-Smirnov test. Direct correlation of both modalities was investigated by temporal mapping of electrical activity in sEMG to DWI repetition interval.

Results: Electrical activities in sEMG and number of visible SMAMs in DWI showed a strong correlation ($\rho = 0.9718$). High accordance between sEMG activities and visible SMAMs in DWI in a near-surface region around sEMG electrodes was achieved. Characteristics of sEMG activities were almost similar under varying magnetic field conditions.

Conclusion: Visible SMAMs in DWI have shown a close and direct relation to concurrent signals recorded by sEMG. MR-related magnetic fields had no significant effects on findings in sEMG. Hence, appearance of SMAMs in DWI should not be considered as imaging artifact or as effects originating from the special conditions of MR examinations. Spatial and temporal distributions of SMAMs indicate characteristics of spontaneous (microscopic) mechanical muscular action at rest. Thus, DWI techniques should be considered as non-invasive tools for studying physiology and pathophysiology of spontaneous activities in resting muscle.

Key Words: Spontaneous Mechanical Activities in Musculature, Surface Electromyography, Diffusion-Weighted Imaging, Incoherent Motion

Introduction

Diffusion-weighted imaging (DWI) enables non-invasive imaging of self-diffusion of water molecules at microscopic levels. DWI is already well established for clinical examinations of stroke patients, for fiber tracking in white matter of the brain, and for tumor staging (1). Sophisticated techniques with variable strengths, timings and orientations of diffusion-sensitizing gradients allow for assessment of microscopic features of tissues in many current investigations (2-5).

DWI also has a crucial role in non-invasive studying of muscle architecture and physiology: Diffusion-tensor imaging (6) enables characterization of microscopic anatomical structures including muscle fiber direction and mean fiber dimensions (7-9). Changes in fractional anisotropy are detectable under varying conditions (10).

While DWI provides insight into diffusion or incoherent motion of water molecules of skeletal musculature, electrophysiological properties can be recorded by electromyography methods. Even simultaneous examinations with MRI and non-invasive version of electromyography utilizing surface electrodes (surface electromyography, sEMG) can be performed with special MR-compatible equipment: First simultaneous measurements have been performed by Hoffmann et al. (11) in order to investigate the influence of fast switching gradient fields in echo planar imaging on the peripheral nerve system and for assessment of related stimulation activation thresholds. A major problem is the influence of gradient switching (with high induced voltages) on recording of very small electrical potential differences on the skin by sEMG. However, suitable methods for removal of related undesired signals in sEMG data have been developed and successfully applied during quantitative functional MRI of the brain and simultaneous isometric contractions of first dorsal interosseus (12) as well as irregular limb motion (13). sEMG is also an established technique for measuring the electromechanical delay between electrical activation and force onset of muscle fibers (stretching of mechanically active components) by fusion with mechanomyography or ultrasound examinations (14, 15). Muscle contractile properties are often measured under active voluntary control or by surface electrode induced potentials (electrically evoked). For active isometric muscle contraction an electromechanical delay of 49.73 ± 7.99 ms has been reported in the literature (14), but it was also reported that electrically stimulated contractions show a significantly shorter electromechanical delay than voluntary contractions (16). Furthermore, each muscular activity has a specific contraction and relaxation time which is probably depending on the composition of muscle fiber types. Contraction and half-relaxation times of single twitches have been determined by electrical stimulation to ensure repeatability of measurements. For m. gastrocnemius medialis around 110 ms (17) have been reported for contraction and half-relaxation time, respectively.

Due to the diffusion-sensitizing gradients with long-lasting diffusion-sensitizing time in between, the DWI technique is well-known to be susceptible to non-diffusional but incoherent motion-induced effects (18-20). Incoherent motion due to vessel enlargement from cardiac pulsation has been reported to cause circular signal voids in the vicinity of large vessels (21, 22). However, signal voids can also occur in

muscle regions with higher distance to large vessels, which cannot be suppressed by electrocardiography triggering (22, 23). These signal voids in DWI can originate from active microscopic incoherent motion of skeletal musculature as reported recently (22-25). This incoherent motion is considered to be an independent source of muscular motion-induced effects recordable by MRI.

In a recent study (23), it was shown that sporadic incoherent motion inside various muscle groups in the lower leg might lead to signal voids in repetitive single-shot diffusion-weighted stimulated echo (26) echo planar imaging. It is assumed that this incoherent motion is caused by unconscious focal spontaneous mechanical activity of the musculature (SMAM). These focal activities are leading to signal voids due to incoherent motion by non-uniform contraction of single muscle fibers or small compartments of muscles groups. SMAMs in DWI have shown random appearance in spatial and temporal domain without strong correlation to different b-values, diffusion-sensitizing direction, cardiac pulsation or patient position (23). Figure 1a/1c show DWI of human calves recorded in time periods without SMAMs and without resulting signal voids, whereas images in Figure 1b/1d clearly exhibit distinct SMAMs in m. gastrocnemius medialis and m. soleus. The underlying processes of the SMAMs are still not fully understood. DWI enables to image these mechanical activities encoded as signal drop in the MRI.

Usually, muscular activation is a consequence of preceding electrical activities measurable by sEMG techniques. However, correlations with electrical activities of SMAM-affected muscle regions have not been studied so far. This work focuses on temporal and spatial relations between spontaneous electrical activity (revealed by sEMG) and SMAMs (visualized by DWI) in healthy volunteers.

In order to examine potential influences of the MR system (static magnetic field, gradient switching, and RF pulses) on spontaneous electrical activity, sEMG measurements were recorded under varying magnetic field conditions. Therefore, sEMG were recorded without the influence of MR magnetic fields, inside the static magnetic field and under MR imaging conditions. In the latter case results of sEMG measurements were fused with concurrent DWI to get insight into the relationship of measurable mechanical and electrical muscle activities.

Methods

Participants and Measurement Procedure

Seven male and one female volunteers (age: 34 ± 13 years, body mass index: 24.8 ± 1.4 kg/m²) participated in the study after giving written informed consent. A potentially strong correlation between sEMG events and visible SMAMs in DWI were expected and thus a small sample size was chosen. Moreover, long lasting time series of data were recorded, which increases the number of spontaneous events in both modalities. The study protocol was approved by the local ethics review board. sEMG examinations started after at least 5 minutes of resting in order to achieve well relaxed musculature of the lower leg. Furthermore, the heel was placed on a soft towel and the foot position was stabilized to prevent leg

movements and to ensure muscular relaxation during longer examination times. The measurement protocol included three sEMG examinations under varying conditions: 1st outside of the MR examination room to reduce possible influences of the magnetic field, 2nd inside the MR bore in the static magnetic field of the scanner (without gradient switching and RF), and 3rd under MRI scanning conditions (static and time-varying magnetic field). Each sEMG examination lasted 480 s and all measurements were executed in the same order without repetition. For subsequent sEMG measurements outside and inside the magnet bore the participants were carried in horizontal position without active movement.

MR setup and sequences

DWI examinations were conducted on a 3 T MR scanner (MAGNETOM Skyra, Siemens Healthcare GmbH, Erlangen, Germany) with a 15-channel Tx/Rx knee-coil. Transverse slices were recorded while the volunteers were comfortably lying in supine position. A prototype DWI single-shot stimulated-echo echo-planar imaging sequence (Siemens Healthcare GmbH, Erlangen, Germany) was utilized (Figure 2a). The sequence parameters were chosen analogous to an earlier protocol reported in (23): matrix size of 64 x 64, field of view (FoV) of 192 x 192 mm², slice-thickness of 6 mm, 6/8 readout, receiver bandwidth (BW) = 2004 Hz/px, echo time TE = 31 ms, repetition time TR = 500 ms, mixing time TM = 145 ms and diffusion-sensitizing time Δ = 157 ms. A b-value of 100 s/mm² was chosen according to previous studies as reported in (23). This b-value leads to easily observable SMAMs in DWI, appearing with complete signal voids. On the other hand, signal intensity of unaffected surrounding muscle is not strongly decreased, since sensitivity to “true diffusion” is relatively weak. Thus, DWI with b = 100 s/mm² show SMAMs with relatively high contrast to surrounding muscle areas.

In former studies SMAMs showed similar spatial and temporal characteristics for all three orthogonal diffusion gradient directions used (23). The signal extinction pattern was nearly independent of the diffusion gradient direction, since incoherent motion components occurred along all spatial axes. Therefore, the diffusion-sensitizing gradient was restricted to the head-feet direction. Taking the 480 s of sEMG into account, a series of 960 repetitive measurements was acquired. For fat suppression a so called spectral attenuated inversion recovery (SPAIR) preparation was chosen. All DWI were acquired at the position with maximum diameter of the right calf. For anatomical referencing T₁-weighted fast spin-echo images at same location with matrix size of 256 x 256, FoV of 192 x 192 mm², slice-thickness of 6 mm, BW of 180 Hz/px, TE = 10 ms, TR = 650 ms and echo train length of 5 were acquired. To determine vessel location, flow-compensated gradient-echo images were acquired at same slice position with matrix size of 288 x 288, FoV of 200 x 200 mm², slice-thickness of 4 mm, BW of 405 Hz/px, TE = 4.6 ms, TR = 650 ms and 15 averages.

sEMG setup

Three bipolar circular-shaped gelled Ag/AgCl electrodes with 8 mm inner diameter were placed on m. gastrocnemius medialis of the right calf with an inter-electrode distance of 2 cm. The m. gastrocnemius medialis was chosen because especially high spontaneous activity had been seen in this region of the

calf as reported in (23) (sEMG electrode placement is depicted in Supporting Figure S1). An eight channel MR-compatible amplifier (BrainAmp ExG MR, Brain Products GmbH, Gilching, Germany) with appropriate recorder software (BrainVision Recorder, Brain Products GmbH, Gilching, Germany) was utilized for sEMG acquisition. The sEMG signal was recorded with a sampling rate of $f_{\text{sampling}} = 5$ kHz, resolution of $0.5 \mu\text{V}$ and dynamic range of ± 16.384 mV. For adequate suppression of signals from the electric power supply, the sEMG signal was notch filtered at 50 Hz. To ensure patient safety by reducing induction voltage, all applied sEMG electrodes have had an incorporated serial resistor $R = 15 \text{ k}\Omega$ (27) and twisted wires (28). To provide an accurate MR gradient distortion correction, the sampling clock of the sEMG equipment was synchronized with the MR gradient clock by manufacturer tools (BrainVision Syncbox, Brain Products GmbH, Gilching, Germany) (29).

Post-processing

sEMG

The distortions in sEMG signals caused by gradient switching were corrected using FACET (Flexible Artifact Correction and Evaluation Toolbox) (30) and EEGLAB (31). The average template method from Van der Meer et al. (13) and artifact residual removal based on Niazy et al. (32, 33) (FMRIB plugin for EEGLAB, provided by the University of Oxford Centre for Functional MRI of the Brain) were utilized for this purpose. Techniques are based on template subtraction according to Allen et al. (34); for template generation epochs with highest correlation were utilized (13). Subsequent artificial residuals were removed by fitting principle components of the signal on an optimal-basis set (PCA-OBS) (32, 33). Narrowband distortions were additionally reduced by notch-filtering. Besides MR-induced artifacts, sEMG signals could also be impaired, if electrodes were placed nearby vessels. Most of signal power of the ballistocardiogram is present below a frequency of 12 Hz (35), thus no effects on spontaneous sEMG activities were assumed. Therefore, a band pass-filter of $f_{\text{bp}} = 20\text{-}500$ Hz was applied for ballistocardiac artifact suppression with additional reduction of high-frequency environmental noise.

Spontaneous aperiodic and biphasic sEMG activities as shown in Figure 2b and Figure 3 were semi-automatically detected with a custom made program in MATLAB (The Mathworks, Inc., Natick, MA, USA). sEMG detections within an amplitude range of $\pm 10 \mu\text{V}$ were discarded (independent of the different magnetic field conditions), since those more random signals are not indicating clear activities in musculature. In a first step, sEMG activities were detected by an implementation of the matched filter method according to Merlo et al. (36, 37). A 10-scale continuous wavelet transform with first order Hermite-Rodriguez polynomial as mother wavelet was utilized. Pulse duration was set to 5-20 ms based on pre-evaluation of the pulse duration of 27 randomly chosen potentials (3 potentials of each participant). Thresholds for activation detection were user-defined for each sEMG channel. sEMG events within a range of 200 ms were considered as one activity. In second step, all detected potential activities were monitored by a human observer to ensure the classification of results.

DWI

SMAMs are causing signal drops in muscle areas of single images of DWI series. Those signal voids were automatically detected and segmented by an self-written MATLAB routine (38). The routine is based on a two-stage detection and refinement segmentation approach: After preprocessing (image scaling and registration), events in DWI were detected in a time-difference representation of DWI (39-42) and subsequently utilized as seeding points for a graph-based segmentation procedure (43, 44). For evaluation, event count maps (ECM) representing the activity of each voxel within a DWI series were calculated. Segmentation and classification results were subsequently controlled.

For visualization, DWI were interpolated on a 512 x 512 matrix size (same for Supporting Animation S1, S2, S3, S4 and S5).

Evaluation of sEMG activity

Bulk movements indicated by high sEMG activity across multiple channels or distinct signal drop across multiple muscle regions/whole muscles were discarded from the evaluation in both modalities.

sEMG activity of resting legs was assessed in terms of overall number of spontaneous sEMG activities for all three different conditions. A non-parametric Friedman test (45) (three paired measurements) in SPSS (IBM Corp., Armonk, USA) was applied for detection of significant differences. To reveal potential intra-individual changes in the temporal distribution of sEMG activities, each sEMG series measured inside MR bore and under imaging condition was compared to the measurement outside of the MR examination room. A two-sample Kolmogorov-Smirnov test (46, 47) with significance level $\alpha = 0.01$ was applied on the inter-event temporal distance (i. e. temporal distance between consecutive sEMG activities) to get insight into the temporal distribution of sEMG events within the time series.

Evaluation of temporal and spatial relations between signal voids in DWI and sEMG

In a first approach, correlations between visible SMAMs in DWI and sEMG signals were assessed by calculating the correlation coefficient between the overall numbers of activities in both modalities. For a more detailed insight, temporal relations between signal voids in DWI and sEMG activities were investigated. For this purpose each sEMG activity was analyzed regarding its time point in the course of the DWI sequence. It is obvious that DWI is only sensitive to incoherent motion taking place in-between switching of diffusion-sensitizing gradients, and therefore not necessarily all SMAMs are resulting in visible signal voids.

Signal amplitudes in single sEMG channels and the distance between the respective sEMG electrode and concurrent signal voids in DWI were evaluated. For that, DWI were registered on anatomical images and the shortest in-plane distance between the boundary of the signal void and the position of the sEMG electrode on the skin in DWI was measured (sEMG electrode location was determined in T₁-weighted spin-echo and gradient-echo anatomical images). The evaluation of the spatial relations between sEMG

activities and visible SMAMs in DWI was performed under consideration of the fact that an sEMG electrode has a limited detection range due to signal attenuation of electrical signals in tissue.

The influence of the time point of sEMG activities with respect to the course of the DWI sequence on the visibility of related SMAMs in DWI was further evaluated. Mapped sEMG activities were analyzed separately for cases with and without related visible SMAMs (images with signal voids) in DWI.

Results

All sEMG measurements (including those inside the MR unit and active DWI recording) led to sufficient quality for reliable evaluation of electrical muscle activity. Only one channel was excluded from evaluation due to large signal distortions (Ch. 2 on subject #1). The maximum allowed signal amplitude ($V_{\max} = \pm 16.384$ mV) of the sEMG amplifier was never exceeded, and so no saturation of the front-end of the sEMG amplifier occurred. Therefore, it was possible to derive an undistorted artifact template from each raw sEMG signal for the correction of MR gradient artifacts. In 45.6 ± 13.0 % of all detected sEMG events the human observer had to intervene due to small residual MR gradient or vibration artifacts. Figure 3 shows an sEMG measurement during one repetition interval in DWI. Time periods with gradient switching in the sequence resulted in very dominant induced voltages in the sEMG with amplitude of up to $2960 \mu\text{V}$. sEMG signal region with low-intensity noise of only $\pm 10 \mu\text{V}$ is highlighted in b) and c). One exemplary spontaneous sEMG activity is clearly visible in this example after MR gradient artifact correction and band pass-filtering at 423 ms with signal amplitude of $27.7 \mu\text{V}$.

Kolmogorov-Smirnov testing of the dependence of sEMG activity distribution on the magnetic field conditions in the three measurements did not indicate significant differences ($P > 0.01$) except for subject #5. Intra-variability across all sEMG measurements was 31.3 ± 16.6 %. The overall activity in sEMG and number of visible SMAMs in DWI are given in Table 1. No significant differences in overall sEMG activity for different magnetic field conditions are detectable by analyzing the three paired measurements with a non-parametric Friedman test (IBM SPSS: mean ranks: 1.38, 2.38, 2.25, Friedman's $Q = 4.750$ and $P = 0.120$). Time points of sEMG activities of each electrode during DWI have not shown prominent temporal clustering within the repetition interval (given in Supporting Figure S2). sEMG activities of two subjects (#5 and #8) with highest and lowest overall number of SMAMs in DWI are depicted in Figure 4a for the three different conditions mentioned above. Clear inter-individual differences regarding the frequency of sEMG events are obvious, whereas different conditions (with and without static, gradient, and RF-magnetic fields) did not lead to marked intra-individual changes. A nearly uniform temporal spread over the entire measurement time of 480 s without any prominent clustering in both subjects is noticeable. The empirical cumulative density functions $F(\Delta t)$ of inter-event time distance Δt of both subjects are depicted in Figure 4b showing only small intra-individual changes.

In Figure 5, sEMG measurements recorded outside of MR examination room during a period of 100 s and ECMs of DWI series (200 repetitions) are depicted for subjects #5 and #8 (time series of DWI for both subjects are illustrated in Supporting Animation S2 and S3). Clear inter-individual differences in the frequency of activities between the subjects are perceptible in both modalities: Figure 5a shows 37 spontaneous sEMG activities within a time interval of 100 s for subject #5 versus only three activities for subject #8 in Figure 5b. The ECM of subject #5 in Figure 5c shows more than 10 activities per voxel in 200 image frames with large SMAM-affected regions. In contrast, ECM of subject #8 in 5d has only small affected regions with few SMAMs at same location in DWI. From Table 1, it can be seen that subjects with higher activity in sEMG outside the MR also had a high activity in DWI (ECM maps of all volunteers are depicted in Supporting Figure S1). Correlation coefficient between both modalities is $\rho = 0.9718$ (sEMG events outside MR room vs. number of visible SMAMs, $P < 0.001$).

Four TR intervals (2 s) of an sEMG measurement with concurrent DWI are demonstrated in Figure 6. sEMG signal recorded on Ch. 3 at m. gastrocnemius medialis shows two activities within this time period. The raw signal of Ch. 3 is depicted additionally in order to provide temporal relation of electrical activity to the DWI sequence. Under the assumption that the DWI sequence is no longer able to encode motion occurring after signal readout, the detection frame for each DWI was set from -175 ms to 325 ms in relation to the TR interval. This region corresponds to the time between diffusion rephasing gradient of previous repetition and diffusion rephasing gradient of current repetition and results in a temporal window of 500 ms. An sEMG activity which was present within repetition no. 118 had a concurrent visible SMAM in DWI. In contrast, an sEMG activity within repetition no. 115 has not resulted in a visible SMAM in DWI. It is also shown exemplarily that intermediate DWI repetitions without activity in sEMG never show SMAM activity in near-surface electrode distance. These findings support following interpretation: Some electrical activities seen in sEMG lead to mechanical responses in musculature taking place during the motion-sensitive period of the DWI sequence, whereas other electrical activities probably lead to SMAMs invisible in DWI, because their temporal course starts and ends outside the motion-sensitive frames of DWI. For a more detailed insight over a longer time interval, Supporting Animation S1 depicts a period of 24 s of concurrent sEMG with DWI of subject #5 for all three electrodes.

The temporal mapping of all sEMG activities from all subjects with (marked in blue) and without (marked in red) visible SMAM in DWI is given in Figure 7a. In total 60.4 % of all sEMG activities can be mapped to an according visible SMAM in DWI, hence 39.6 % showed no visible SMAM. Most sEMG activities occurring directly after motion-sensitizing period don't lead to visible SMAMs in DWI. Based on this, the probability that an sEMG activity results in visible SMAM in DWI in relation to the time point of occurrence is depicted for subjects #1, #5 and all subjects in Figure 7b (probability calculation was restricted on those two subjects due to the requirement of sufficient amount of data). Temporal distance was determined as time between sEMG activity and onset of diffusion rephasing gradient

(end of motion-sensitive period). With a higher temporal distance than 300-350 ms (respectively 143-193 ms to onset of diffusion dephasing) the probability that an sEMG activity lead to visible SMAM in DWI is markedly reduced.

The relation between amplitude of sEMG activity and distance between SMAMs in DWI and sEMG electrode location is depicted in Figure 8. The regions of skin and subcutaneous tissue (in average 6.51 mm over all subjects) as well as the noisy region within $\pm 10 \mu\text{V}$ are separated. It can be seen that with increasing distance between the sEMG electrode and the boundary of signal void in DWI the measured maximum voltage at the electrode decreases from up to $120 \mu\text{V}$ to $10\text{-}20 \mu\text{V}$; however, also events with smaller amplitudes were observed with rather low distance to the electrode position.

In Figure 9, the relative share of visible SMAMs in DWI with detectable sEMG activity is illustrated. Relative counts of SMAMs were determined in assumed circular detection areas around sEMG electrodes starting from a radius of 10 mm to 100 mm for each subject in Figure 9a, and as average over all subjects in Figure 9b. Nearly all SMAMs visible in DWI within a small distance of 10-15 mm to the sEMG electrodes also showed an electrical activity in sEMG recordings. In a region of 15 mm around electrode location the relative amount of SMAMs in DWI with concurrent sEMG activities was between 69.7-100 %, with an average accordance of 91.3 ± 10.9 %. A decrease to 36.1 ± 16.7 % was found for increasing the electrode distance to 30 mm.

Discussion

Electrical activities measured by sEMG of the lower leg in healthy volunteers at rest were found to be not markedly affected by outer static or variable magnetic fields as present during MRI examinations. This statement is statistically supported by non-parametric Friedman test and Kolmogorov-Smirnov despite one exceptional subject (#5). However, intra-variability regarding the number of sEMG events of subject #5 (26.8 %) was smaller compared to the overall intra-variability considering all subjects (31.3 %). Moreover, longer lasting sEMG measurements from one volunteer have revealed a variability of about 24 %, thus high intra-variability is to be expected in intra-individual examinations. SMAMs could be well visualized in all volunteers by signal voids in DWI with relatively low b-values (approx. 100 s/mm^2), and those signal voids show a strong correlation to preceding detectable sEMG activities. Observed signal voids in DWI in a region of 15 mm around sEMG electrodes had related sEMG activities in 91.3 ± 10.9 % of all cases (total number of SMAMs in this region was 133 in 8 volunteers). If peripheral nerve stimulation or other MR-induced motion caused additional mechanical activity, an increased activity level would have been measurable with potential temporal clustering at regions of MR switching (11). Since small mechanical activities of lower leg musculature indicated by signal voids in DWI are 1st closely related to electrical activities visible by sEMG and 2nd those electrical activities are not significantly influenced by static or variable magnetic fields, it is supposed that the conditions of

MR examinations including gradient switching are not causing the phenomenon of SMAMs and related signal voids in DWI.

Not all electrical activities indicated by sEMG led to SMAMs visible in DWI. This finding can be at least partly explained by the temporal sensitivity characteristics of the DWI sequence to motion. In the applied DWI sequence the incoherent motion-sensitive time between both sensitizing gradients amounted to 157 ms, whereas the rest of the TR interval of 343 ms was insensitive. Furthermore, only incoherent motion of muscle fibers which is not completely reversed in-between motion-sensitizing gradients will lead to signal voids in DWI. This limited sensitivity of DWI to muscular activities was reflected by the distributions of sEMG activities with and without visibility of SMAMs in DWI, which were found to be unbalanced over the repetition interval of DW sequence. Most sEMG activities with a temporal distance up to 300-350 ms till the end of motion-sensitive period led to visible SMAMs in DWI, thus the minimal duration of a SMAM should be about 143-193 ms (time to onset of incoherent motion-sensitive period).

Spatial and temporal relations between matching activities in sEMG and visible SMAMs in DWI were analyzed: It was found that the voltages of sEMG activities were decreasing for higher distances between the electrode location on the skin surface and the muscular area with signal void. This finding is in consensus to an expected decay of electrical signals inside tissue (48). Due to marked attenuation of electrical signals in tissue sEMG inherently enables only local detection coverage. Regarding this, a detection range of about 10-35 mm was reported for activities with 40 μ V peak-peak amplitude depending on the number of innervating fibers (48). That implies that electrical signals of SMAMs in deeper muscle regions, e. g. in m. soleus or m. tibialis posterior, should be more difficult or even impossible to detect using sEMG equipment. The evaluation of the accordance between visible SMAMs in DWI and sEMG activities confirms this expected behavior: In deeper muscular areas less SMAMs visible in DWI have a relation to concurrent measurable sEMG activities. For distances ranging 15-30 mm, the relative share of SMAMs in DWI with preceding detectable sEMG activity drops from 91.3 ± 10.9 % to 36.1 ± 16.7 %. Within this spatial region, the fascia between m. soleus and m. gastrocnemius medialis seems to be responsible for an increased electrical attenuation (distance from electrode to fascia for all subjects in average 27.1 ± 4.7 mm in our measurements). Mechanical muscular activity behind this fascia was often not paralleled by detectable sEMG signals, and subjects with rather high mechanical activity in deeper muscle regions (as revealed by ECMs) sometimes showed relatively low activity in sEMG. In contrast, accordance between both modalities was especially high for small distances up to 15 mm between sEMG electrodes and visualized mechanical activities: nearly all SMAMs visualized in DWI were also visible in electrical signal the neighboring sEMG electrode. Nevertheless, a few signal voids in DWI due to SMAMs did obviously not show preceding detectable sEMG signals. One possible explanation for this finding is that “active” muscle contractions occur in remote regions of the same muscle

outside of the sEMG detection range. Since muscles and their fibers are relatively long, incoherent motion can be possibly transferred from the “active” area to other regions along the muscle axis causing the mentioned phenomenon. It was found in earlier (DWI only) measurements that the extension of signal voids along the fiber direction is often much larger compared to the perpendicular view (23).

Whether sEMG events are leading to signal voids in DWI or not is mainly depending on the delay from the electrical event to the onset of the mechanical activity and on the duration of the incoherent motion. Mechanical activities starting directly after a motion-sensitive interval in DWI are possibly relaxed before the next motion-sensitive period in the DWI sequence starts, and thus were not visible in DWI. No reliable data for durations and time courses of spontaneous microscopic muscular activities (SMAMs) are available, but it is likely that typical principles of electro-mechanical coupling in musculature are also valid in those cases. It should be mentioned that electromechanical delay is usually measured during repeated voluntary controlled muscle exercise or by electrical stimulation. However, time courses might be different between intentional activities with strong parallel electrical stimulation by nerves and spontaneous muscle activities with their clearly weaker electrical representation.

The physiological background of SMAMs is still not fully clear. On the one hand, spontaneous minor membrane depolarization of myocytes have been reported to cause weak continuous fluctuations in the EMG of healthy subjects at rest, but this phenomenon does not seem to cause mechanical activities. On the other hand, action potentials of motor neurons are known as common stimulus for the excitation of larger muscle areas (motor units, comprising hundreds of myocytes in the calf muscles). Fasciculations are visible but unintentional contractions that occur spontaneously in healthy subjects or subjects affected by movement disorders, motor neuron diseases or system diseases (49). These fasciculations are caused by repetitive activation by motor units (50) leading to electric potentials in sEMG with a peak-to-peak amplitude up to 500 μV (51). Due to the near-surface detection radius of sEMG-electrodes and non-noticeable muscular contractions under the skin of the subjects, the activities are potentially smaller compared to fasciculations, but larger than single fiber contractions, which are difficult to be detected by sEMG (52). The impression of spatial extensions of SMAMs suggests that at least a considerable number of muscle fibers (possibly many fibers belonging to one motor unit innervated by one motor neuron) were activated for muscular contraction. It seems that the reported “SMAMs” are in-between these two well-known levels of muscular activity, and it is still unknown where SMAMs originate and how motor neurons are involved.

It seems likely that temporal and spatial patterns of SMAMs are influenceable by both, neurogenic and myopathic diseases. If the hypothesis holds true that spontaneous action potentials in single motor neurons are causing SMAMs, the frequency and distribution of those events possibly reflect spontaneous depolarization of motor neurons. Thus, detection of SMAMs could be helpful for assessment of early stages of motor neuron diseases. However, these statements are speculative.

This study is limited due to the restriction of measurements to a constant b-value, diffusion-sensitizing time Δ and repetition time TR. The diffusion-sensitizing time Δ affects the sensitivity of the DW sequence to tissue incoherent motion effects (22) and hence the ability to image SMAMs (53). As reported in (23), a reduced repetition time increases the chance to image SMAMs at the same location in consecutive DWI and hence should affect the overall ability to detect SMAMs in general, but prolonged repetition time increases SNR (Supporting Animation S4/S5 in contrast to S2/S3). To investigate the overall influence of each sequence parameter onto the ability of the DWI sequence to image SMAMs systematic studies on many SMAM events have to be carried out. Results have to be analyzed statistically due to the uniqueness of each single event.

This study shows spontaneous microscopic muscle contractions with electrically measurable potentials without outer nerve stimulation. Fusion of sEMG and DWI enables estimation of the temporal delay between onset of sEMG activities and resulting incoherent motion without electrical stimulation.

It should be noted that an electromyogram is known to show nearly lacking electrical activity of skeletal muscle at rest. Only spontaneous electrical discharges have been reported to result in small electrical signals in sEMG of the healthy human musculature. The nature of the spontaneous local incoherent motions is still not totally clarified. However, this report shows that there are clear spatial and temporal correlations between small electrical potentials measurable by sEMG and microscopic incoherent muscular motion measurable by DWI.

Conclusion

The study shows that most spontaneous activities of human musculature in the lower leg, especially in superficial areas, are detectable by both diffusion-weighted MRI and surface EMG. Both techniques can be applied simultaneously enabling a good coverage of electrical and mechanical activities, including their spatial and temporal relations. In our setup, it was shown that the MR system itself had no significant influence on the occurrence of spontaneous activities in sEMG. According to this and the overall strong correlation between sEMG and visible SMAMs, no influence of MR-related circumstances on the spontaneous electrical and mechanical activity is to be expected. Due to the fact that recorded SMAMs are not related to MR imaging artifacts and showing a tight correlation to electrophysiological processes, the topic of SMAMs should not be considered as MR imaging artifact but rather as new interesting opportunity to assess resting muscle activity non-invasively.

Acknowledgements

We thank Nerea Irastorza-Landa, Andrea Sarasola-Sanz, Boris Kotchoubey and Farid Shiman from the Institute for Medical Psychology and Behavioural Neurobiology, University of Tübingen, for their valuable technical support on this project.

References

- [1] Le Bihan D, Johansen-Berg H. Diffusion MRI at 25: exploring brain tissue structure and function. *Neuroimage* 2012;61(2):324-41.
- [2] Jiang X, Li H, Xie J, McKinley ET, Zhao P, Gore JC, Xu J. In vivo imaging of cancer cell size and cellularity using temporal diffusion spectroscopy. *Magn Reson Med* 2016.
- [3] Jiang X, Li H, Xie J, Zhao P, Gore JC, Xu J. Quantification of cell size using temporal diffusion spectroscopy. *Magn Reson Med* 2016;75(3):1076-85.
- [4] Reynaud O, Winters KV, Hoang DM, Wadghiri YZ, Novikov DS, Kim SG. Pulsed and oscillating gradient MRI for assessment of cell size and extracellular space (POMACE) in mouse gliomas. *NMR Biomed* 2016;29(10):1350-63.
- [5] Reynaud O, Winters KV, Hoang DM, Wadghiri YZ, Novikov DS, Kim SG. Surface-to-volume ratio mapping of tumor microstructure using oscillating gradient diffusion weighted imaging. *Magn Reson Med* 2016;76(1):237-47.
- [6] Basser PJ, Mattiello J, LeBihan D. MR diffusion tensor spectroscopy and imaging. *Biophys J* 1994;66(1):259-67.
- [7] Basser PJ, Pajevic S, Pierpaoli C, Duda J, Aldroubi A. In vivo fiber tractography using DT-MRI data. *Magn Reson Med* 2000;44(4):625-32.
- [8] Damon BM, Ding Z, Anderson AW, Freyer AS, Gore JC. Validation of diffusion tensor MRI-based muscle fiber tracking. *Magn Reson Med* 2002;48(1):97-104.
- [9] Heemskerk AM, Damon BM. Diffusion Tensor MRI Assessment of Skeletal Muscle Architecture. *Curr Med Imaging Rev* 2007;3(3):152-160.
- [10] Schwenzer NF, Steidle G, Martirosian P, Schraml C, Springer F, Claussen CD, Schick F. Diffusion tensor imaging of the human calf muscle: distinct changes in fractional anisotropy and mean diffusion due to passive muscle shortening and stretching. *NMR Biomed* 2009;22(10):1047-53.
- [11] Hoffmann A, Faber SC, Werhahn KJ, Jager L, Reiser M. Electromyography in MRI--first recordings of peripheral nerve activation caused by fast magnetic field gradients. *Magn Reson Med* 2000;43(4):534-9.
- [12] van Duinen H, Zijdwind I, Hoogduin H, Maurits N. Surface EMG measurements during fMRI at 3T: accurate EMG recordings after artifact correction. *Neuroimage* 2005;27(1):240-6.
- [13] van der Meer JN, Tijssen MA, Bour LJ, van Rootselaar AF, Nederveen AJ. Robust EMG-fMRI artifact reduction for motion (FARM). *Clin Neurophysiol* 2010;121(5):766-76.
- [14] Begovic H, Zhou GQ, Li T, Wang Y, Zheng YP. Detection of the electromechanical delay and its components during voluntary isometric contraction of the quadriceps femoris muscle. *Front Physiol* 2014;5:494.
- [15] Cavanagh PR, Komi PV. Electromechanical delay in human skeletal muscle under concentric and eccentric contractions. *Eur J Appl Physiol Occup Physiol* 1979;42(3):159-63.

- [16] Zhou S, Lawson DL, Morrison WE, Fairweather I. Electromechanical delay in isometric muscle contractions evoked by voluntary, reflex and electrical stimulation. *Eur J Appl Physiol Occup Physiol* 1995;70(2):138-45.
- [17] Vandervoort AA, McComas AJ. A comparison of the contractile properties of the human gastrocnemius and soleus muscles. *Eur J Appl Physiol Occup Physiol* 1983;51(3):435-40.
- [18] Le Bihan D, Turner R. Intravoxel incoherent motion imaging using spin echoes. *Magn Reson Med* 1991;19(2):221-7.
- [19] Norris DG. Implications of bulk motion for diffusion-weighted imaging experiments: effects, mechanisms, and solutions. *J Magn Reson Imaging* 2001;13(4):486-95.
- [20] Gallichan D, Scholz J, Bartsch A, Behrens TE, Robson MD, Miller KL. Addressing a systematic vibration artifact in diffusion-weighted MRI. *Hum Brain Mapp* 2010;31(2):193-202.
- [21] Merboldt KD, Hanicke W, Frahm J. Diffusion imaging using stimulated echoes. *Magn Reson Med* 1991;19(2):233-9.
- [22] Karampinos DC, Banerjee S, King KF, Link TM, Majumdar S. Considerations in high-resolution skeletal muscle diffusion tensor imaging using single-shot echo planar imaging with stimulated-echo preparation and sensitivity encoding. *NMR Biomed* 2012;25(5):766-78.
- [23] Steidle G, Schick F. Addressing spontaneous signal voids in repetitive single-shot DWI of musculature: spatial and temporal patterns in the calves of healthy volunteers and consideration of unintended muscle activities as underlying mechanism. *NMR Biomed* 2015;28(7):801-10.
- [24] Steidle G, Eibofner F, Schick F. Quantitative diffusion imaging of adipose tissue in the human lower leg at 1.5 T. *Magn Reson Med* 2011;65(4):1118-24.
- [25] Szeverenyi N, Bydder G. Fasciculation MR Imaging (faMRI) of the Lower Leg. In Proceedings of the 24th Annual Meeting of ISMRM. 2016. Singapore. #4528.
- [26] Steidle G, Schick F. Echoplanar diffusion tensor imaging of the lower leg musculature using eddy current nulled stimulated echo preparation. *Magn Reson Med* 2006;55(3):541-8.
- [27] Lemieux L, Allen PJ, Franconi F, Symms MR, Fish DR. Recording of EEG during fMRI experiments: patient safety. *Magn Reson Med* 1997;38(6):943-52.
- [28] Goldman RI, Stern JM, Engel J, Jr., Cohen MS. Acquiring simultaneous EEG and functional MRI. *Clin Neurophysiol* 2000;111(11):1974-80.
- [29] Mandelkow H, Halder P, Boesiger P, Brandeis D. Synchronization facilitates removal of MRI artefacts from concurrent EEG recordings and increases usable bandwidth. *Neuroimage* 2006;32(3):1120-6.
- [30] Glaser J, Beisteiner R, Bauer H, Fischmeister FP. FACET - a "Flexible Artifact Correction and Evaluation Toolbox" for concurrently recorded EEG/fMRI data. *BMC Neurosci* 2013;14:138.
- [31] Delorme A, Makeig S. EEGLAB: an open source toolbox for analysis of single-trial EEG dynamics including independent component analysis. *J Neurosci Methods* 2004;134(1):9-21.

- [32] Iannetti GD, Niazy RK, Wise RG, Jezzard P, Brooks JC, Zambreau L, Vennart W, Matthews PM, Tracey I. Simultaneous recording of laser-evoked brain potentials and continuous, high-field functional magnetic resonance imaging in humans. *Neuroimage* 2005;28(3):708-19.
- [33] Niazy RK, Beckmann CF, Iannetti GD, Brady JM, Smith SM. Removal of FMRI environment artifacts from EEG data using optimal basis sets. *Neuroimage* 2005;28(3):720-37.
- [34] Allen PJ, Josephs O, Turner R. A method for removing imaging artifact from continuous EEG recorded during functional MRI. *Neuroimage* 2000;12(2):230-9.
- [35] Grouiller F, Vercueil L, Krainik A, Segebarth C, Kahane P, David O. A comparative study of different artefact removal algorithms for EEG signals acquired during functional MRI. *Neuroimage* 2007;38(1):124-37.
- [36] Lo Conte LR, Merletti R, Sandri GV. Hermite expansions of compact support waveforms: applications to myoelectric signals. *IEEE Trans Biomed Eng* 1994;41(12):1147-59.
- [37] Merlo A, Farina D, Merletti R. A fast and reliable technique for muscle activity detection from surface EMG signals. *IEEE Trans Biomed Eng* 2003;50(3):316-23.
- [38] Schwartz M, Steidle G, Martirosian P, Yang B, Schick F. Graph-based segmentation of signal voids in time series of diffusion-weighted images of musculature in the human lower leg. In *Proceedings of the 24th Annual Meeting of ISMRM*. 2016. Singapore. #1923.
- [39] Salvado O, Bourgeat P, Tamayo OA, Zuluaga M, Ourselin S. Fuzzy classification of brain MRI using a priori knowledge: weighted fuzzy C-means. In *IEEE 11th International Conference on Computer Vision*. 2007. Rio de Janeiro, Brazil.
- [40] Bezdek JC. *Pattern Recognition with Fuzzy Objective Function Algorithms*. 1981, New York: Springer US.
- [41] Dunn J. A fuzzy relative of the ISODATA process and its use in detecting compact, well-separated clusters. *J Cybernetics* 1974;3(3):32-57.
- [42] Iglewicz BH, D.C. *Volume 16: How to Detect and Handle Outliers*. 1993, Milwaukee, United States: ASQC Quality Press.
- [43] Grady L. Random Walks for Image Segmentation. *IEEE Trans Pattern Anal Mach Intell* 2006;28(11):1768-1783.
- [44] Grady L. *The Graph Analysis Toolbox: Image Processing on Arbitrary Graphs*. 2003: Boston University.
- [45] Friedman M. The Use of Ranks to Avoid the Assumption of Normality Implicit in the Analysis of Variance. *J Am Stat Assoc* 1937;32(200):675-01.
- [46] Massey FJ. The Kolmogorov-Smirnov Test for Goodness of Fit. *J Am Stat Assoc* 1951;46(253):68-78.
- [47] Miller LH. Table of Percentage Points of Kolmogorov Statistics. *J Am Stat Assoc* 1956;51(273):111-121.

- [48] Fuglevand AJ, Winter DA, Patla AE, Stashuk D. Detection of motor unit action potentials with surface electrodes: influence of electrode size and spacing. *Biol Cybern* 1992;67(2):143-53.
- [49] Leite MA, Orsini M, de Freitas MR, et al. Another Perspective on Fasciculations: When is it not Caused by the Classic form of Amyotrophic Lateral Sclerosis or Progressive Spinal Atrophy? *Neurol Int* 2014;6(3):5208.
- [50] Engel AG, Franzini-Armstrong C. *Myology*. 2 ed. 1994, New York: McGraw-Hill.
- [51] Van der Heijden A, Spaans F, Reulen J. Fasciculation potentials in foot and leg muscles of healthy young adults. *Electroencephalogr Clin Neurophysiol* 1994;93(3):163-8.
- [52] Keller SP, Sandrock AW, Gozani SN. Noninvasive detection of fibrillation potentials in skeletal muscle. *IEEE Trans Biomed Eng* 2002;49(8):788-95.
- [53] Schwartz M, Steidle G, Martirosian P, Yang B, Schick F. Temporal and spatial characteristics of signal voids in repetitive acquisitions of the human lower leg using spin-echo vs. stimulated echo diffusion-weighted imaging. In *Proceedings of the 33th Annual Scientific Meeting of the ESMRMB*. 2016. Vienna, AT. #695.

Tables

Table 1: Number of spontaneous activities in each measurement for all three different environmental conditions and both modalities: 1st) outside MR room, 2nd) inside MR bore with static magnetic field and 3rd) under imaging conditions. Non-parametric Friedman test shows no significant differences (IBM SPSS: mean ranks: 1.38, 2.38, 2.25, Friedman's $Q = 4.750$ and $P = 0.120$). Number of SMAMs in DWI for all volunteers shows strong correlation to activities in sEMG outside MR room ($\rho = 0.9718$, $P < 0.001$).

Subject	#1	#2	#3	#4	#5	#6	#7	#8
Number of sEMG events (outside MR room)	112	5	28	29	160	6	37	12
Number of sEMG events (inside MR bore)	144	11	42	53	176	28	47	11
Number of sEMG events (imaging condition)	176	15	34	55	259	18	30	9
Number of visible SMAM in DWI	297	37	127	168	466	56	83	20

List of Captions

Figure 1: Four DWI recorded at the right calf of two different subjects. DWI in b) and d) show distinct signal voids in m. soleus and m. gastrocnemius medialis in contrast to DWI in a) and c).

Figure 2: MR sequence scheme and sEMG signal. a) Diffusion-weighted stimulated echo MR sequence with diffusion-sensitizing time $\Delta = 157$ ms. Within the diffusion-sensitizing time, the sequence is sensitive to incoherent motion. b) Period of 25 s sEMG measurement recorded on the m. gastrocnemius medialis at rest showing clear spontaneous activities.

Figure 3: Elimination of sEMG signal distortions in a period of 500 ms (one repetition interval) concurrent sEMG and DWI measurement. a) Raw sEMG signal with gross MR switching artifacts. b) MR gradient corrected sEMG signal shows slow moving artifacts with rather small artifact residuals. c) sEMG signal after band pass-filtering (region of $\pm 10 \mu\text{V}$ highlighted in gray). A spontaneous sEMG activity is perceptible in b) and c) (marked with an asterisk).

Figure 4: Temporal distributions of spontaneous sEMG activities under varying magnetic field conditions. a) Time points of sEMG activities for subject #5 and #8 on the overall measurement time. b) Empirical cumulative density functions $F(\Delta t)$ of inter-event time distance Δt for same subjects.

Figure 5: Period of 100 s surface EMG (sEMG) measurement recorded outside the MR room for subject #5 in a) and subject #8 in b). Distinct differences are perceptible regarding number of spontaneous sEMG activities. ECM of both volunteers for a DWI series of 200 repetitions in c) and d) shows same trend (exemplary sEMG events are highlighted for each channel).

Figure 6: sEMG signal recorded at electrode Ch. 3 during four TR intervals (2 s) with concurrent DW images (repetition 115-118). Artifact corrected sEMG signal at Ch. 3 is depicted at top with two spontaneous sEMG activities. Raw signal is given at the bottom. Red box indicates the detection frame (-175 ms to 325 ms) for one DWI acquisition. Two sEMG activities are perceptible; however, only one SMAM in DWI is visible.

Figure 7: Temporal distribution of sEMG activities for all subjects during the whole measurement time mapped on repetition interval (TR = 500 ms) of DWI sequence in a). All time points of sEMG activities with SMAM in DWI are marked in blue, and without SMAM in DWI in red. Most sEMG activities occurring directly after motion-sensitizing period don't lead to visible SMAMs in DWI. b) Probability of sEMG to result in a visible SMAM in DWI in relation to the time between sEMG activity and end of motion-sensitizing period (onset of diffusion rephasing gradient). Courses are depicted for subjects #1 and #5. Solid line represents probability for all subjects.

Figure 8: sEMG amplitude of spontaneous activity over the distance (measured in imaging plane) between SMAM in concurrent DWI and sEMG electrode location. Event-free regions are indicated as skin

with subcutaneous tissue and amplitude range of $\pm 10 \mu\text{V}$, which was excluded from evaluation. Reduced potentials of SMAMs measured by sEMG occur for increased distance between SMAM and electrode position.

Figure 9: Relative amount of SMAMs in DWI, which are showing activities in concurrent sEMG measurements. Due to limited measurable detection range of each sEMG electrode (due to signal attenuation), the assumed detection range is increased in steps of 5 mm for all volunteers in a) and in average b). The diagrams show a decrease of SMAMs in accordance with increasing of the SMAM to electrode distance.

Supporting Animation S1: sEMG measurement during a period of 24 s with concurrent DWI. All three artifact corrected electrodes with an assumed detection radius of 25 mm (circle in DWI) are depicted. Bottom signal equals raw data signal. Change in circle color indicates sEMG activity of the corresponding electrode (temporal shift between detection frame and DWI sequence (-125-375 ms) has to be considered).

Supporting Animation S2: DWI time series of subject #5 during a period of 24 s. Distinct signal voids are visible in several image frames and different muscle regions, (mainly in m. soleus and m. gastrocnemius medialis). Note that signal voids often show high distance to pulsation sources like vessels.

Supporting Animation S3: DWI time series of subject #8 during a period of 24 s. In contrast to subject #5, rather rare spontaneous activities are recordable.

Supporting Animation S4: DWI time series of an older experiment with longer repetition time (TR = 1000 ms) showing clear signal voids in several muscle regions.

Supporting Animation S5: DWI time series of an older experiment with longer repetition time (TR = 1000 ms) of a subject, which shows rather less spontaneous activities in contrast to Supporting Animation S4.

Supporting Figure S1: SMAM activity maps and sEMG electrode placement. Summed SMAM activities over the whole DWI series (event count map – ECM) for all volunteers showing clear inter-individual differences regarding active muscle region and number of overall occurrences.

Supporting Figure S2: Time points of sEMG activities within repetition interval of DWI sequence for all subjects.

Figure 1

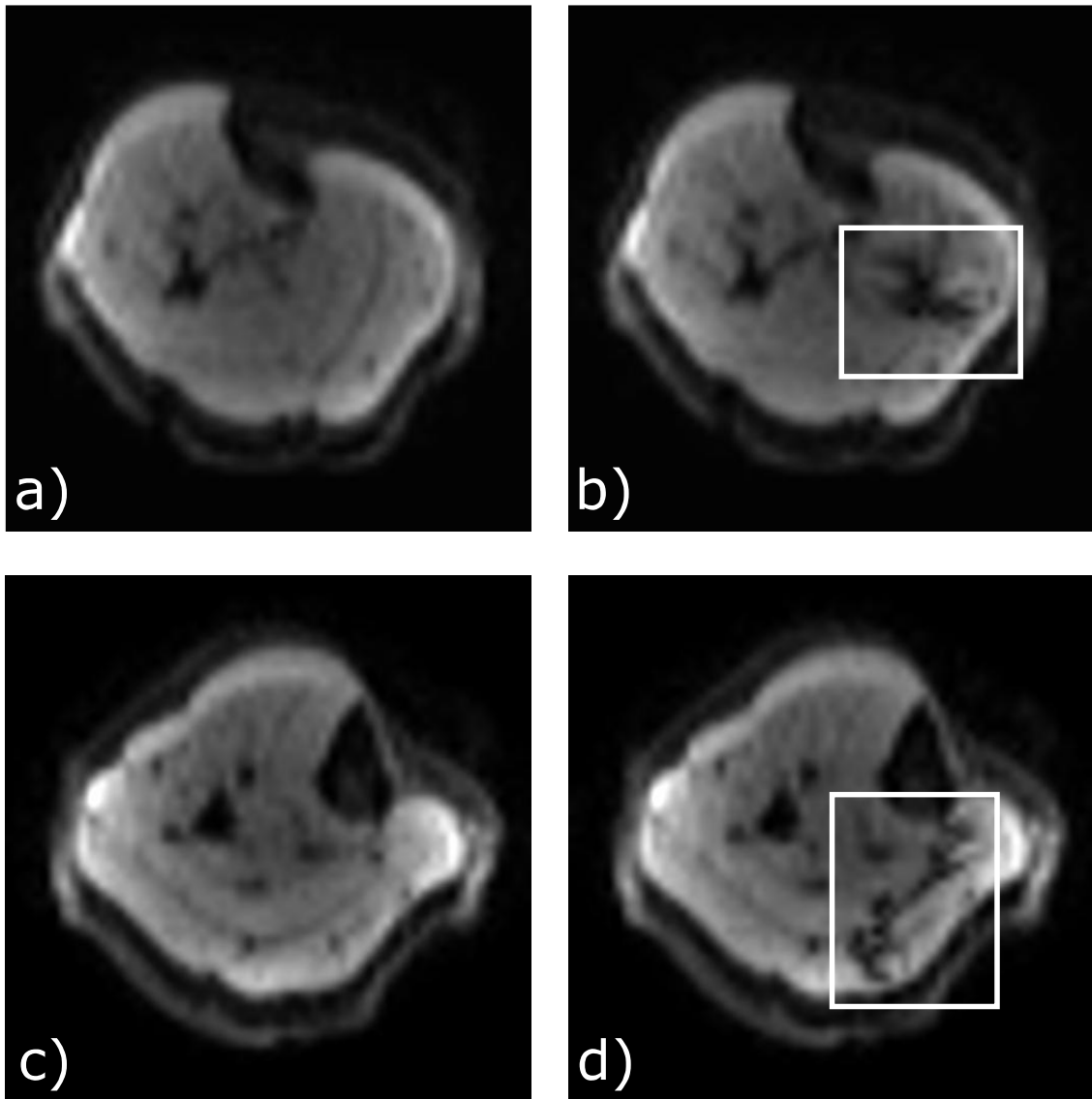


Figure 2

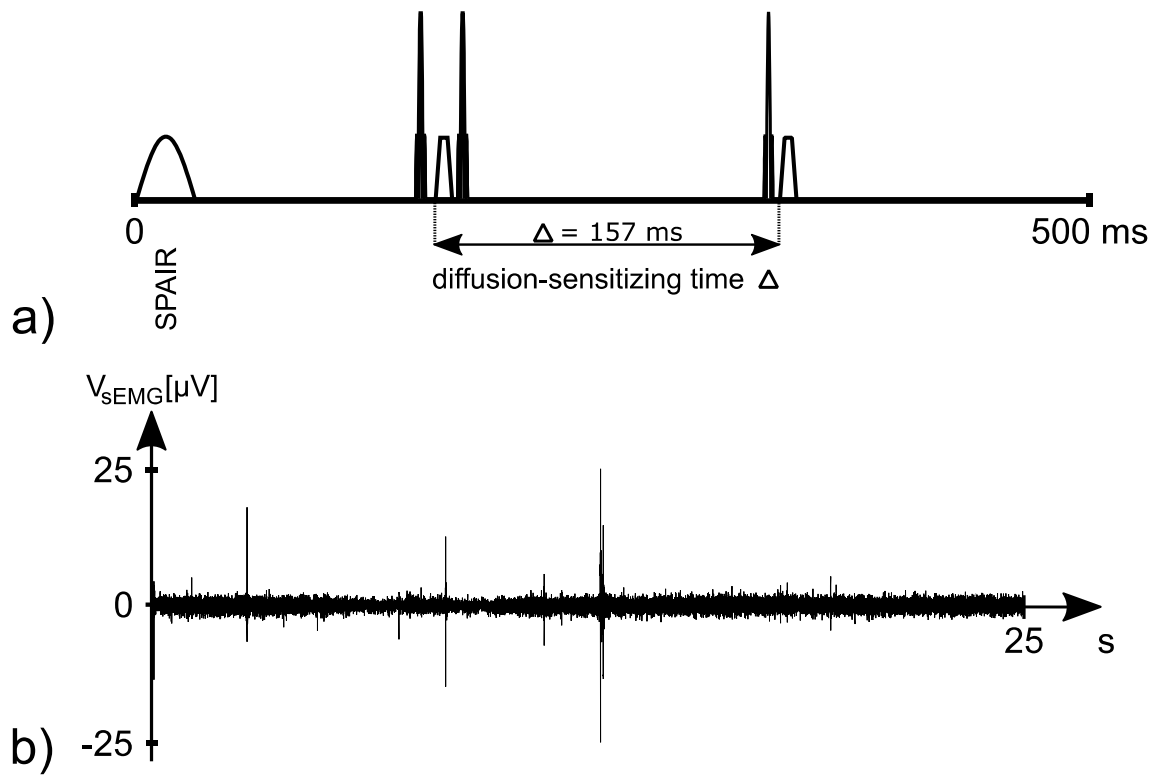


Figure 3

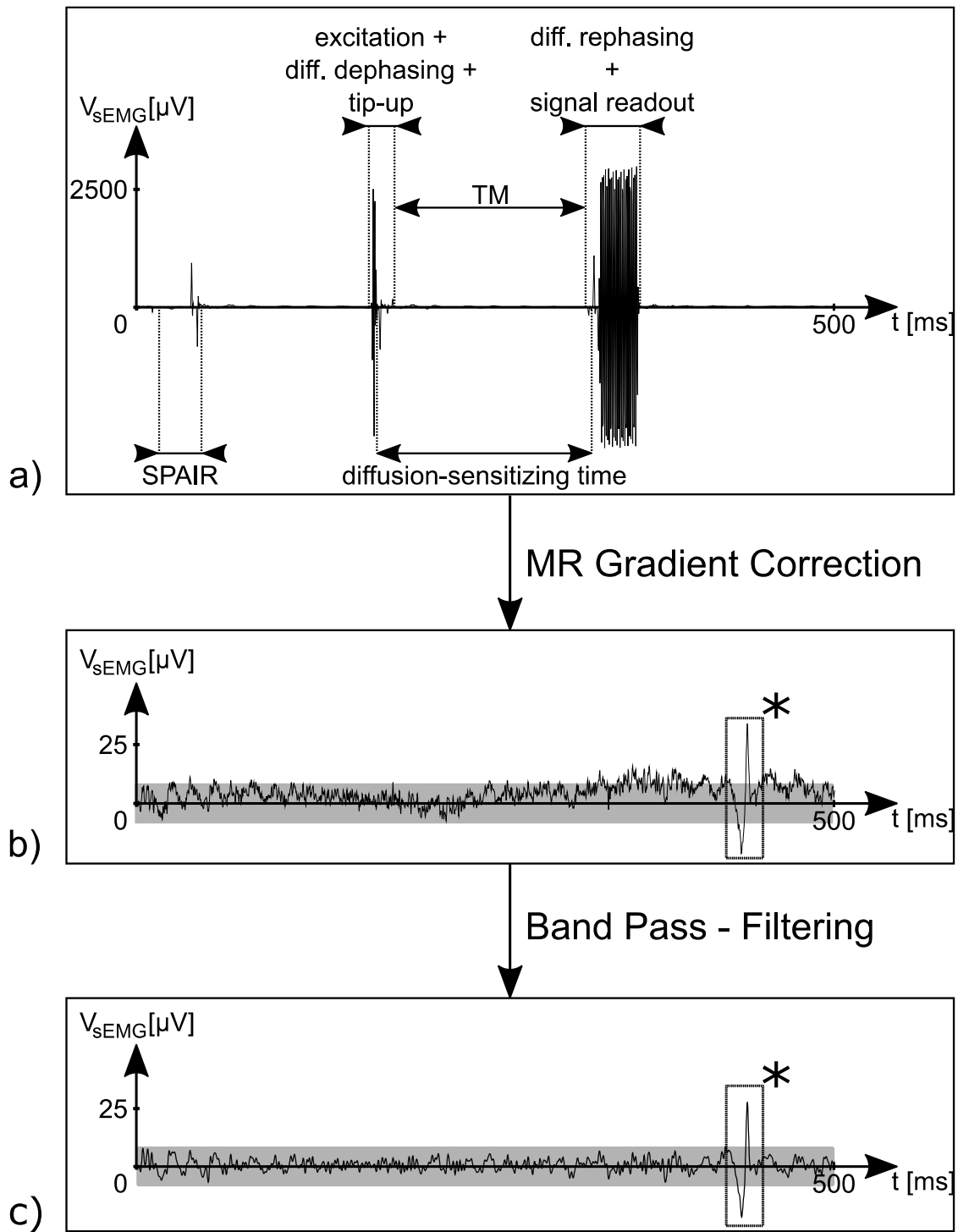


Figure 4

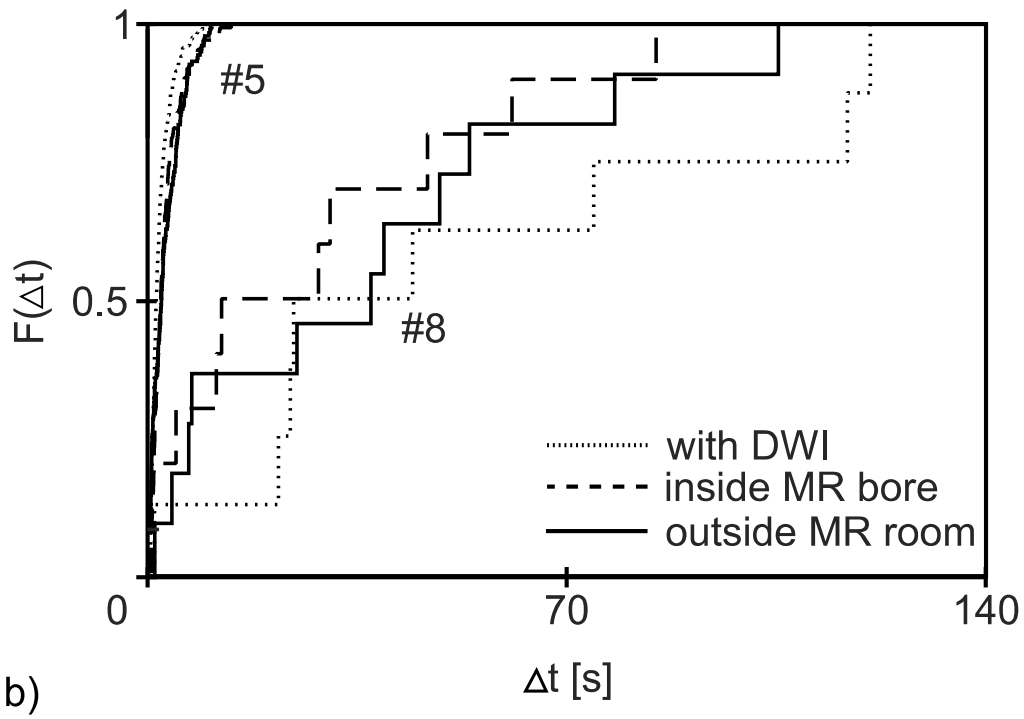
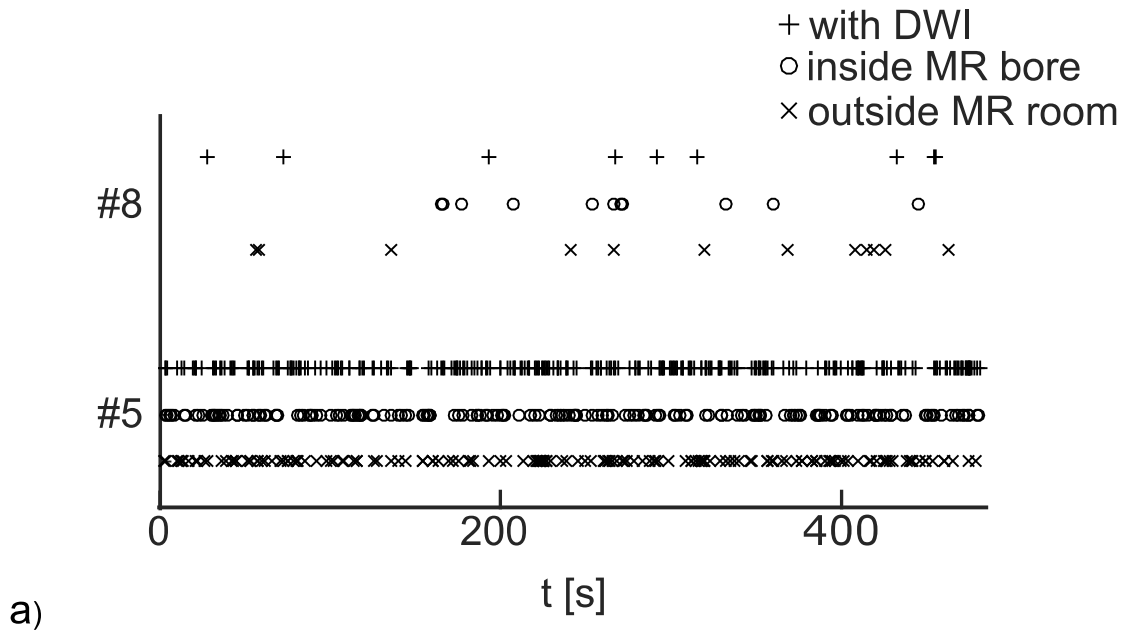


Figure 5

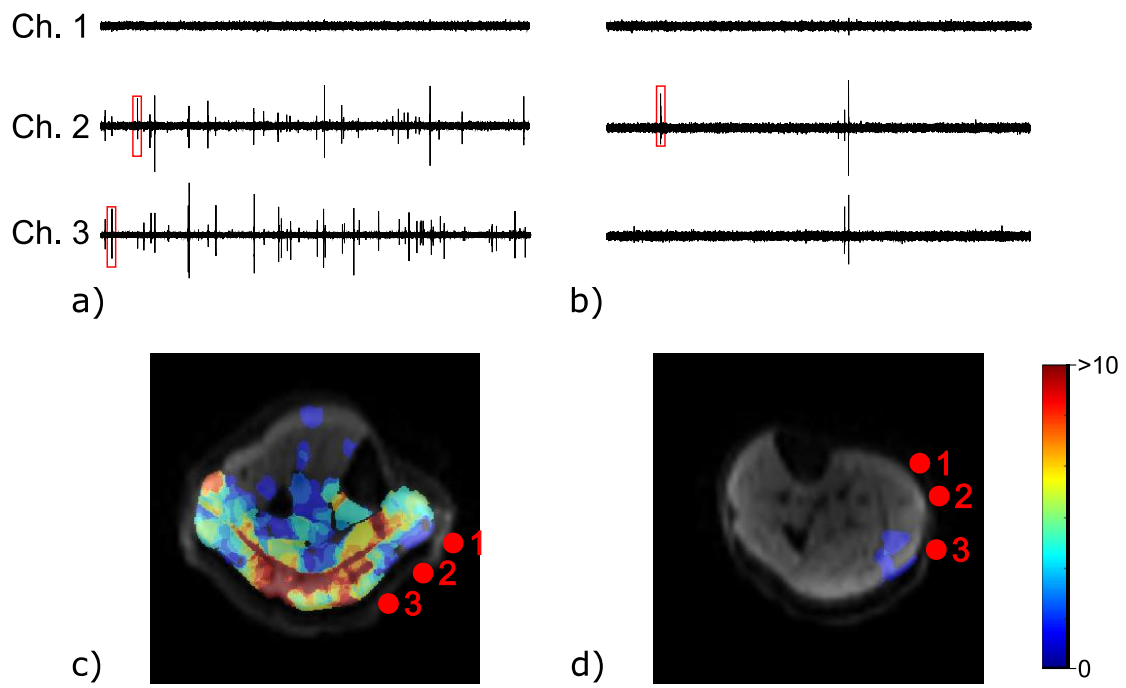


Figure 6

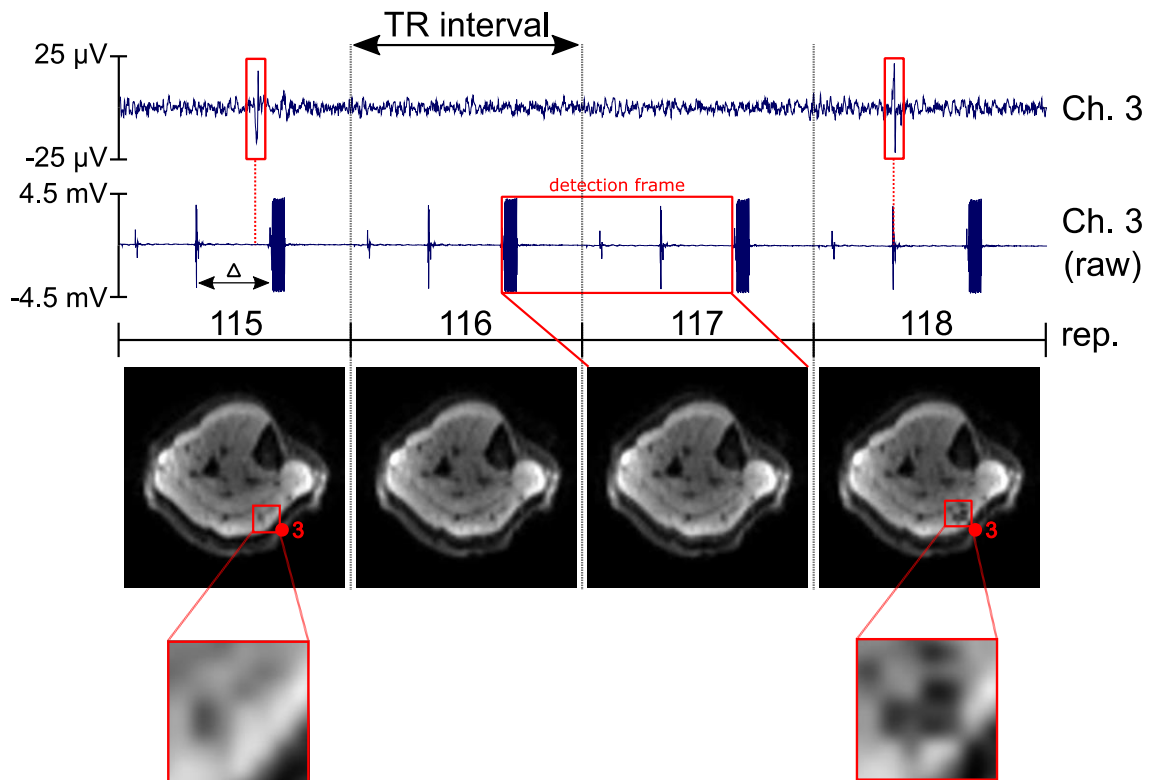
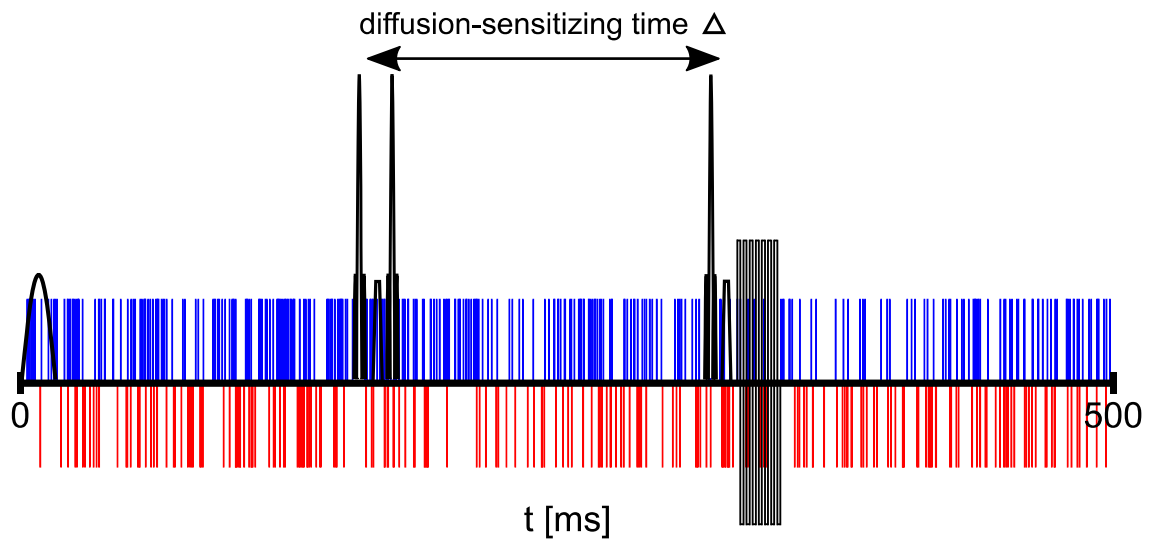


Figure 7





-  EMG event with SMAM in DWI
-  EMG event without SMAM in DWI

Figure 8

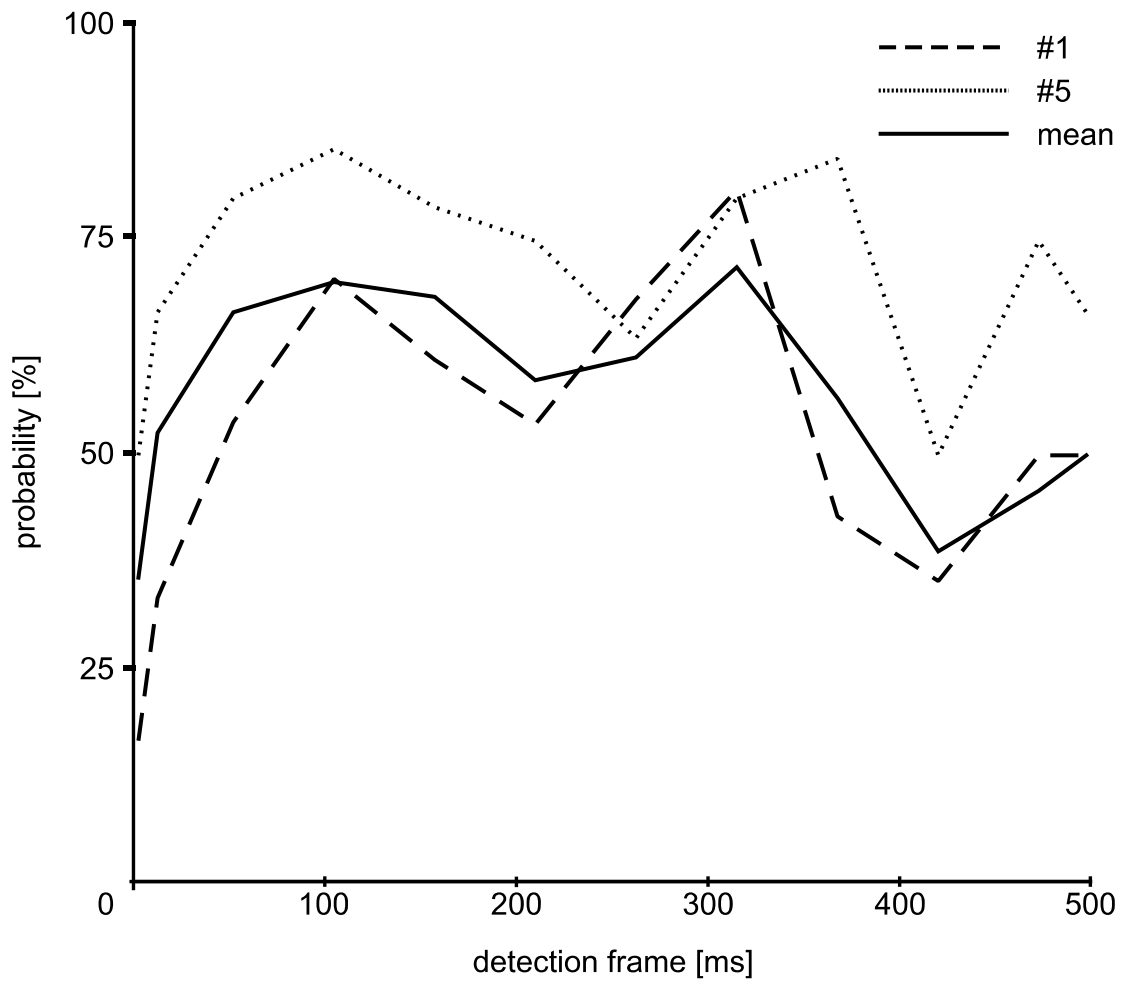


Figure 9

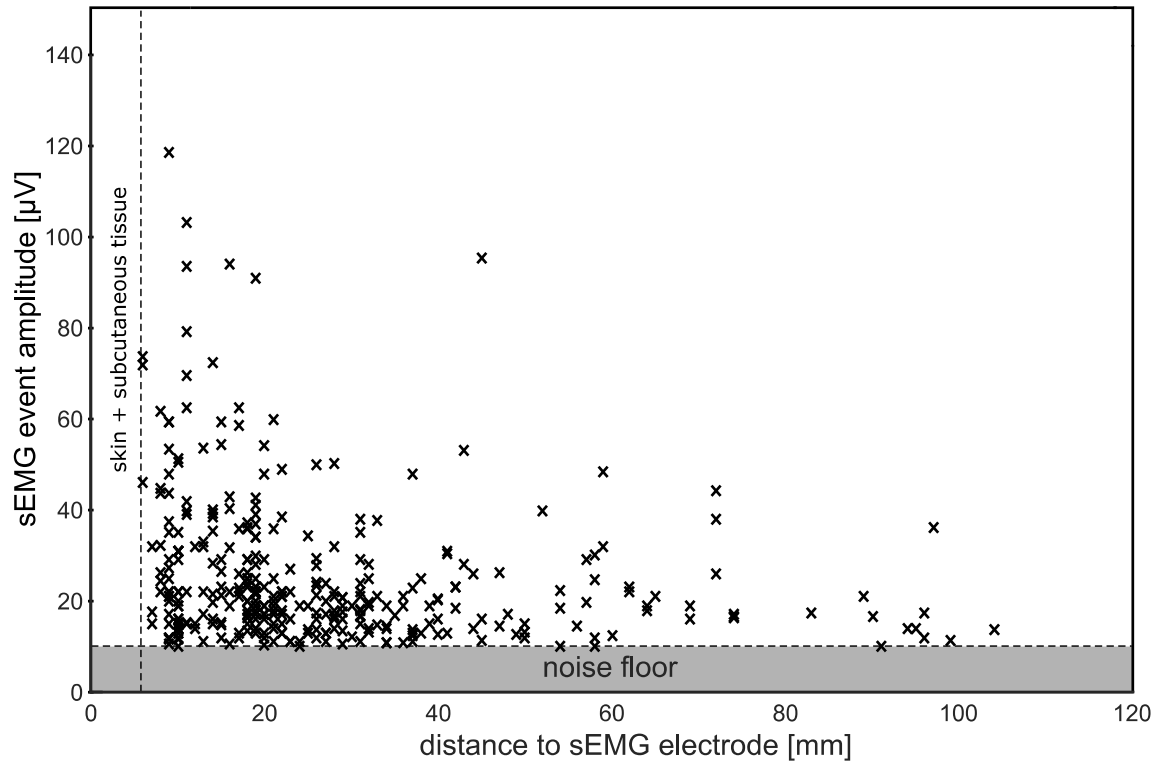
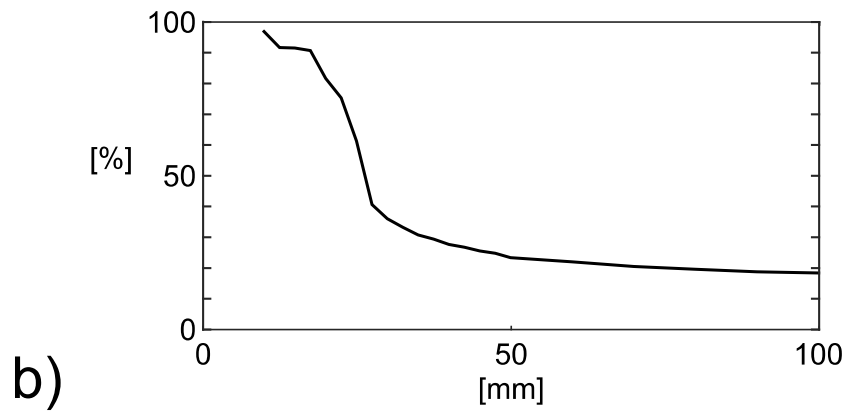
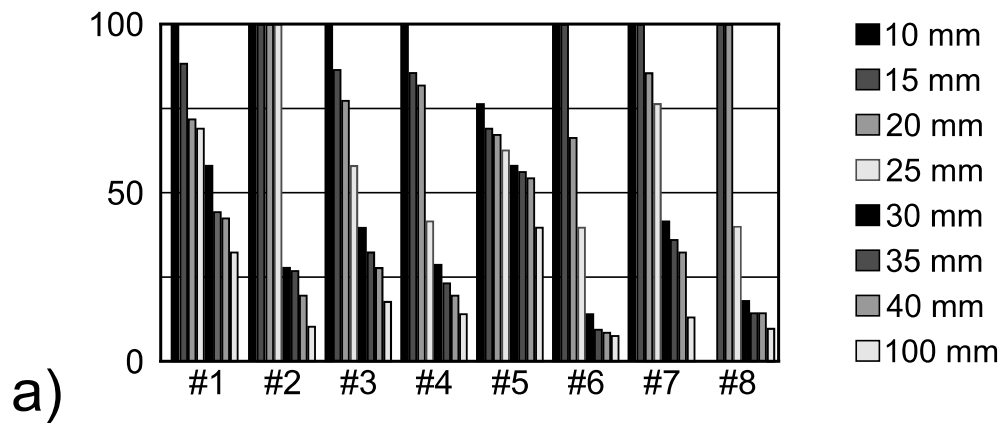
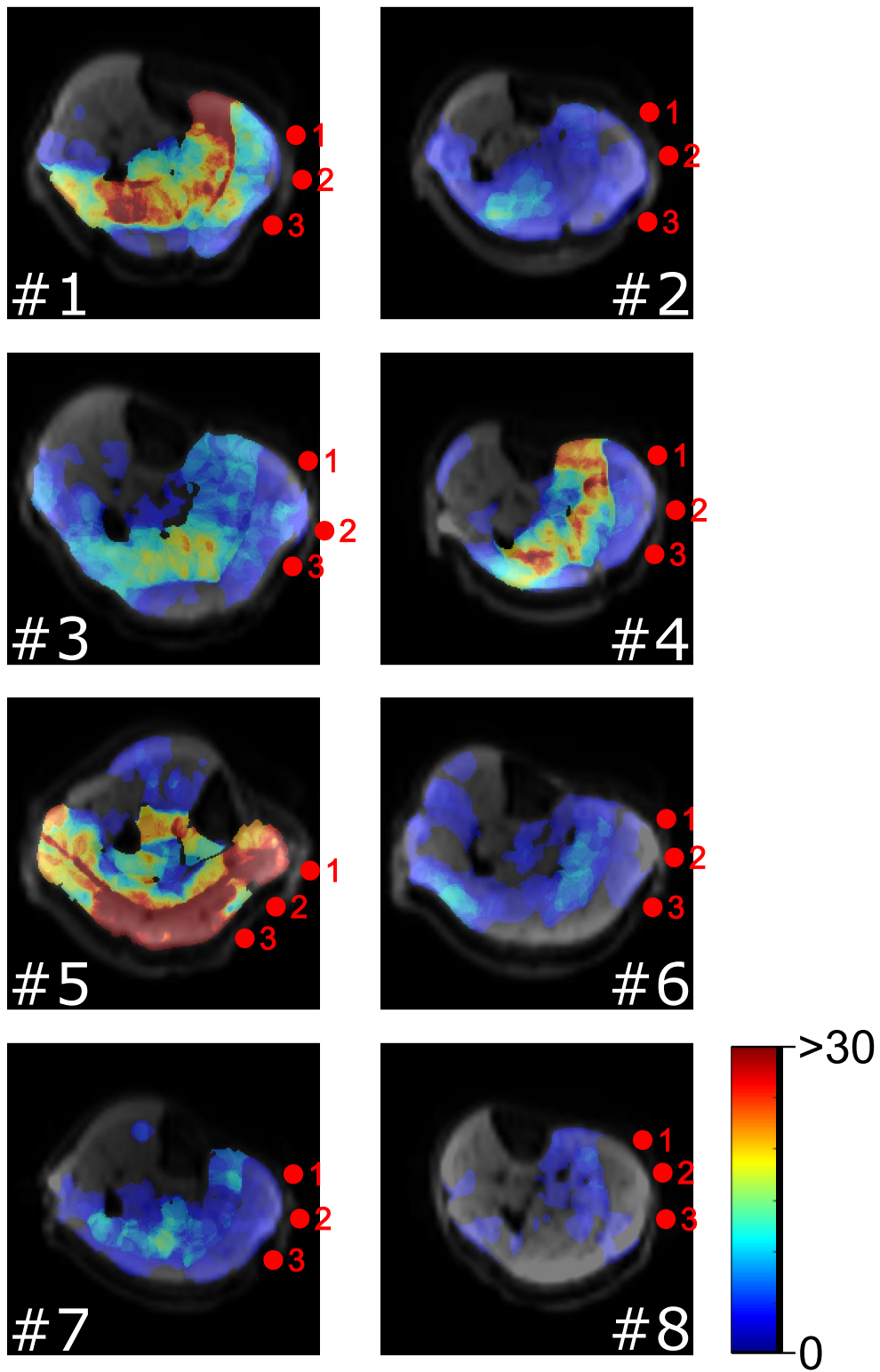


Figure 10



Supporting Figure 1



Supporting Figure 2

